Journal of Petroleum Exploration and Production Technology (2024) 14:1521–1537
https://doi.org/10.1007/s13202-024-01777-9

ORIGINAL PAPER-PRODUCTION ENGINEERING

Experimental data-driven model development for ESP failure diagnosis based on the principal component analysis

Youngsoo Song[1] · Sungjun Jun[1,2] · Tan C. Nguyen[3] · Jihoon Wang[1,3]

Received: 3 September 2022 / Accepted: 28 February 2024 / Published online: 30 March 2024

Abstract

The reliable diagnosis of electrical submersible pump (ESP) failure is a vital process for establishing of the optimal production strategies and achieving minimum development costs. Although traditional ammeter charts and nodal analysis are commonly used for ESP failure diagnosis, the techniques have limitations, as it requires manpower and is difficult to diagnose the failure in real-time. Therefore, in this study, ESP failure diagnosis was performed using the principal component analysis (PCA). First, 11 types of 9,955 pieces of data were acquired from a newly constructed ESP experimental system for 300 days. During the experimental period, ESP failure occurred twice with a significant drop in performance: first on day 112 and second on day 271. The PCA model was constructed with the 8,928 pieces of normal status data and tested with the 1,027 pieces of normal and failure status data. Three principal components were extracted from the measured data to identify the patterns of the normal and failure status. Based on the logistic regression method to analyze the efficiency of the PCA model, it was found out that the developed PCA model showed an accuracy of 93.3%. Therefore, the PCA model was found to be reliable and effective for the ESP failure diagnosis and performance analysis.

Keywords Electrical submersible pump · Experimental system · Failure diagnosis · Principal component analysis

List of symbols

Greek letter

ΔP	Pressure difference (kPa)

Latin letters

E	Residual matrix
N	Number of principal components
n	Sample size
P	Loading matrix
p	Number of original parameters
Q	Interquartile range
r_{xy}	The Pearson correlation coefficient
S	Scaling factor
T	Score matrix
t	Number of time steps
X	Input matrix
x	Target parameter
$\bar{x}$	Mean value of the target parameter
x_i	Individual sample point indexed with $\bar{x}$
y	Target parameter
$\bar{y}$	Mean value of the target parameter
y_i	Individual sample point indexed with $\bar{y}$

Abbreviations

CAHM	Computer-assisted history matching
CFRP	Carbon fibre reinforced plastics
ESP	Electrical submersible pump
NDT	Non-destructive testing
OLT	Optical lock-in thermography
PCA	Principal component analysis
PC	Principal component

✉ Jihoon Wang
jihoonwang@hanyang.ac.kr

[1] Department of Earth Resources and Environmental Engineering, Hanyang University, Seoul 04763, South Korea

[2] Digital & Integration, SLB, Seoul 03157, South Korea

[3] Petroleum and Natural Gas Engineering Department, New Mexico Institute of Mining and Technology, Socorro, NM 87801, USA

Introduction

The artificial lift method is required when the reservoir does not have enough energy to naturally produce oil and gas at the desired rates (Bates et al. 2004; Kolawole et al. 2019; AlJuboori et al. 2020; Al-Janabi and Al-Fatlawi 2022; Syed et al. 2022a). The electrical submersible pump

(ESP) is one of the most common artificial lift methods, which is efficient and reliable for pumping large volumes of fluids (Refai et al. 2013; Seczon and Sagalovskiy 2013; Ballarini et al. 2017; Guindi et al. 2017; Hamzah et al. 2017; Fakher et al. 2021). More than 60.0% of the world's oil is produced by ESP systems (Dunham 2013; Ratcliff et al. 2013; Nguyen 2020) and, over 90.0% of offshore wells use ESP to pump out oil and water to the surface. Although ESPs are fairly reliable, their failures, which are caused by many factors, such as high-gas volumes, produced solids, high temperature, and corrosive environments, occur without precursors (Gupta et al. 2016a). Once failure occurs, the replacement costs with the production loss during the maintenance can be significant (Vandevier 2010). Moreover, in case of unexpected ESP failure, many losses occur during the replacement preparation process (Gupta et al. 2016b). Previous studies have shown that the cost of lost production can be up to $3 million, and the cost of intervention can be up to $1 million per well per year (Carrillo 2013).

To minimize these losses, over the past few decades, improvements have been made in ESP sensors, supervisory controls, data acquisition systems, and remote terminal units for ESP failure diagnosis (Abdelaziz et al. 2017). The major variables related to ESP include the flow rates, pump intake/discharge pressures, motor current and voltage, temperatures, and vibration, and with each variable possessing a normal range. Once deviations from this range are detected, it can be regarded as an abnormal state or a malfunction of the ESP system (Alamu et al. 2020).

Using an ammeter chart is the fastest and simplest ESP diagnostic tool and is still the most widely used method. However, since engineers must visit the wellsite, human costs are required (Bates et al. 2004). This method measures and records the motor current as a function of time on a circular chart (Fig. 1) (Takacs 2017). Since the ammeter chart method relies solely on the motor current, integrated analysis is quite restricted (Peng et al. 2021). The nodal analysis method has been adopted to describe the change in ESP performance and to determine patterns for common ESP failures such as a broken shaft, blockage at pump intake, or an increase in watercut (Awaid et al. 2014). However, the nodal analysis is inapplicable for real-time investigation.

It has been recently discovered that machine learning methods can analyze measured data during operation to identify patterns for real-time abnormally detection, failure diagnosis, production optimization, forecasting, and reduction of uncertainty in asset management (Stone 2007; Syed et al. 2022a). Insuasty et al. (2017) analyzed the applicability of the tensor-based approach by parameter estimation of computer-assisted history matching (CAHM) in the channelized reservoirs. They found that using this approach required only 0.6% of the original amount of information was required to reconstruct the channels properly, while the dimensionality reduction method required 63.0%. When performing CAHM with parameter estimation in the channelized reservoirs, they revealed that utilizing the

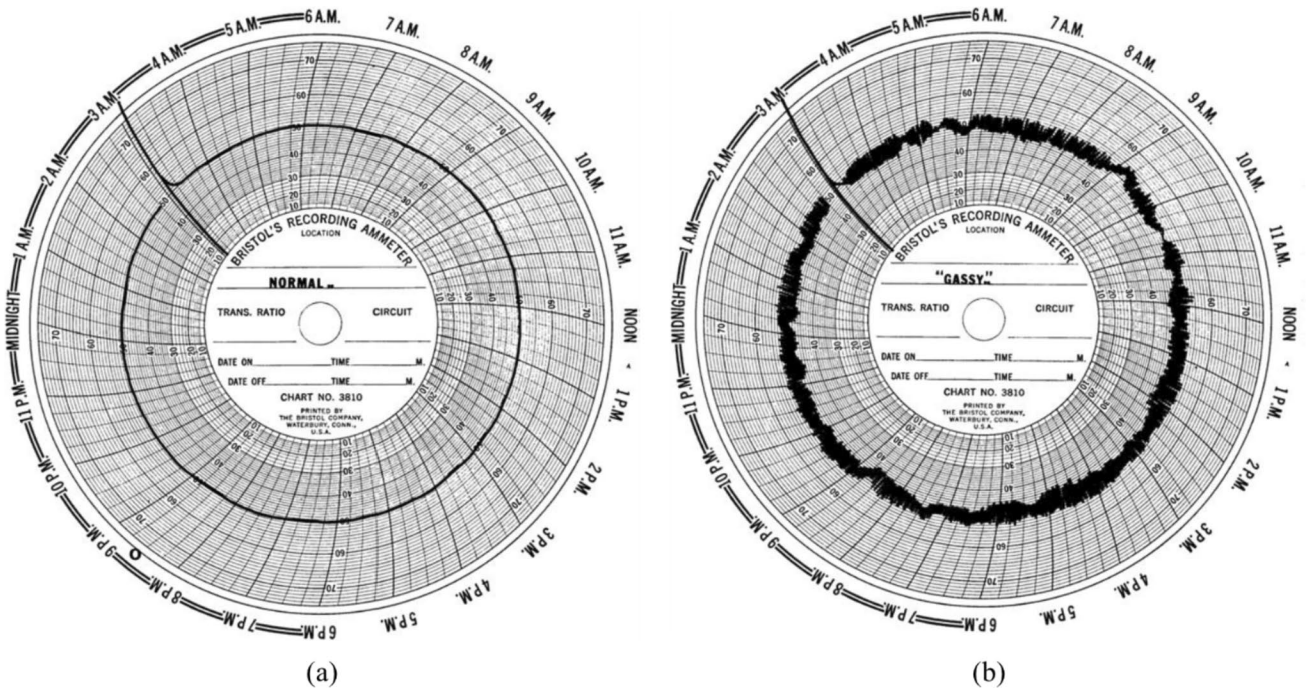

Fig. 1 Example of an ammeter chart in **a** normal operation and **b** free gas production (Takacs 2017)

tensor-based approach yielded better prediction results than the dimensionality method. Syed et al. (2022b) developed a complex tight oil reservoir model by applying a low-rank tensor decomposition method for dimensionality reduction. They dealt with the problems such as huge dataset management and missing data generation using the low-rank tensor decomposition. Additionally, they also presented the applicability of the low-rank tensor decomposition method by effectively improving the computational power. Guo et al. (2015) presented a binary classification model for ESP failure diagnosis, based on the support vector machine method and showed the applicability of the machine learning method for the ESP failure prediction. Andrade Marin et al. (2019) analyzed 165 cases using the random forest method to obtain high accuracy and recall values of ESP failure prediction. Although these machine learning methods can effectively monitor ESP failure diagnosis, their accuracy might be low due to data complexity, as all variables need to be analyzed.

Research adopting the principal component analysis (PCA) method has recently been conducted for multi-variable problems to reduce the dimensions of the target data and creates a new set of principal components (PCs) for more reliable data analysis and visualization (Carobene et al. 2022). The interdependencies in the target data are used to develop a PCA model, which reduces the dimensionality of the variables through the application of linear combinations and the creation of new PCs. With just a few PCs, the PCA model can analyze the entire system, making the process much easier. PCA has the advantage of increasing training time efficiency in machine learning algorithms by removing correlated variables, and it can help overcome the overfitting problems that occur when there are many variables (Phillips et al. 2005; Asadi et al. 2010). In addition, it can be easily visualized by converting it to low-dimensional data through PCA (Carobene et al. 2022). Conversely, PCA has the limitation that data normalization is essential before performing PCA to avoid biased results (Sapra 2010). Also, principal components try to reflect the information in the data as much as possible, but some information might be missed (Li et al. 2008). Although the PCA method may miss useful information when extracting PCs, it has been adopted in various fields and verified the applicability (Gottumukkal and Asari 2004; Salo et al. 2019; Singh et al. 2022). Thus, the PCA method is widely used to find patterns in high-dimensional data and to reduce the dimensionality for integrated data analysis (Peng et al. 2020). Sophian et al. (2003) evaluated the applicability using the PCA method for pulsed Eddy current non-destructive testing (NDT). The authors reduced the dimensionality of the acquired signals through the PCA method and extracted relevant variables to effectively classify the defects. They found out that the performance of classification using the PCA method was better than the conventional method using the response peak characteristics. Oliveira et al. (2021) proposed a transfer learning approach with a U-net neural network used in characteristics of network structures in microscopy for segmenting optical lock-in thermography (OLT) images of carbon fibre reinforced plastics (CFRP) plates with impact damages. After training and testing this model with OLT images, the authors compared the performance between the U-net neural network model and the PCA method. While the performance of the U-net neural network was better, the PCA model also exhibited good performance, especially when the damage was barely visible. In addition, several authors have adopted the PCA method for the predictive analytics of ESP failure diagnosis. Abdelaziz et al. (2017) suggested that PCA has the potential to be adopted as a tool to identify dynamic changes in ESP systems. The authors built different PCA models for each facility to evaluate its applicability. Gupta et al. (2016c) applied the PCA and the multivariate Hotelling T-square statistic to sensor data from ESPs. The data contained 22 variables for the ESP operation, which was then reduced to six principal components after PCA. Although the studies adopting the PCA method have employed data obtained from the field for more practical applications, there are still limitations due to data quality. Field data, normally extracted from the various devices including downhole gauges, motor controllers, and surface gauges is often incomplete, inconsistent, and of low quality (Andrade Marin et al. 2019).

Therefore, this study analyzed the applicability of the PCA method for the ESP failure diagnosis and performance analysis based on the consistent and reliable data obtained from a newly constructed ESP experimental system. A total of 11 variables, including pressure, vibration, acoustic amplitudes, and temperature were measured for 300 days, and a PCA model was constructed to diagnose the ESP failure and to analyze its performance. The proposed PCA model can be effectively implemented for ESP failure diagnosis, and appropriate remedial actions can be taken promptly, which improves development strategies.

Experimental system

To obtain and to analyze signals during the normal and abnormal status of an ESP, the ESP testing system was built in New Mexico Tech. The experimental system comprised a 20 stage ESP, a 50-hp 480-V motor, a gas liquid separator, a liquid tank, gas and liquid flow meters, gas and liquid control valves, pressure and temperature sensors, and a transmitter.

All of the raw data including the pressure, temperature, acoustic amplitude, and vibration signals were recorded using the National Instrument CompactRIO model NI 9148 and LabVIEW. A photograph and the schematic diagram of the system are shown in Figs. 2 and 3, respectively.

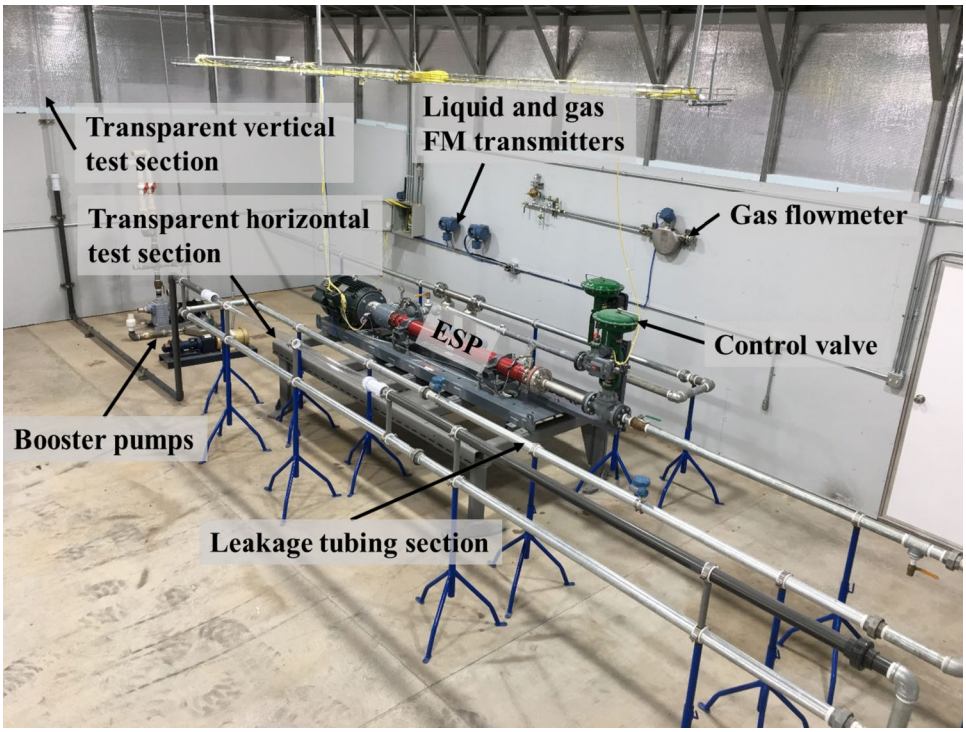

Fig. 2 The ESP testing system in New Mexico Tech (Chu et al. 2021)

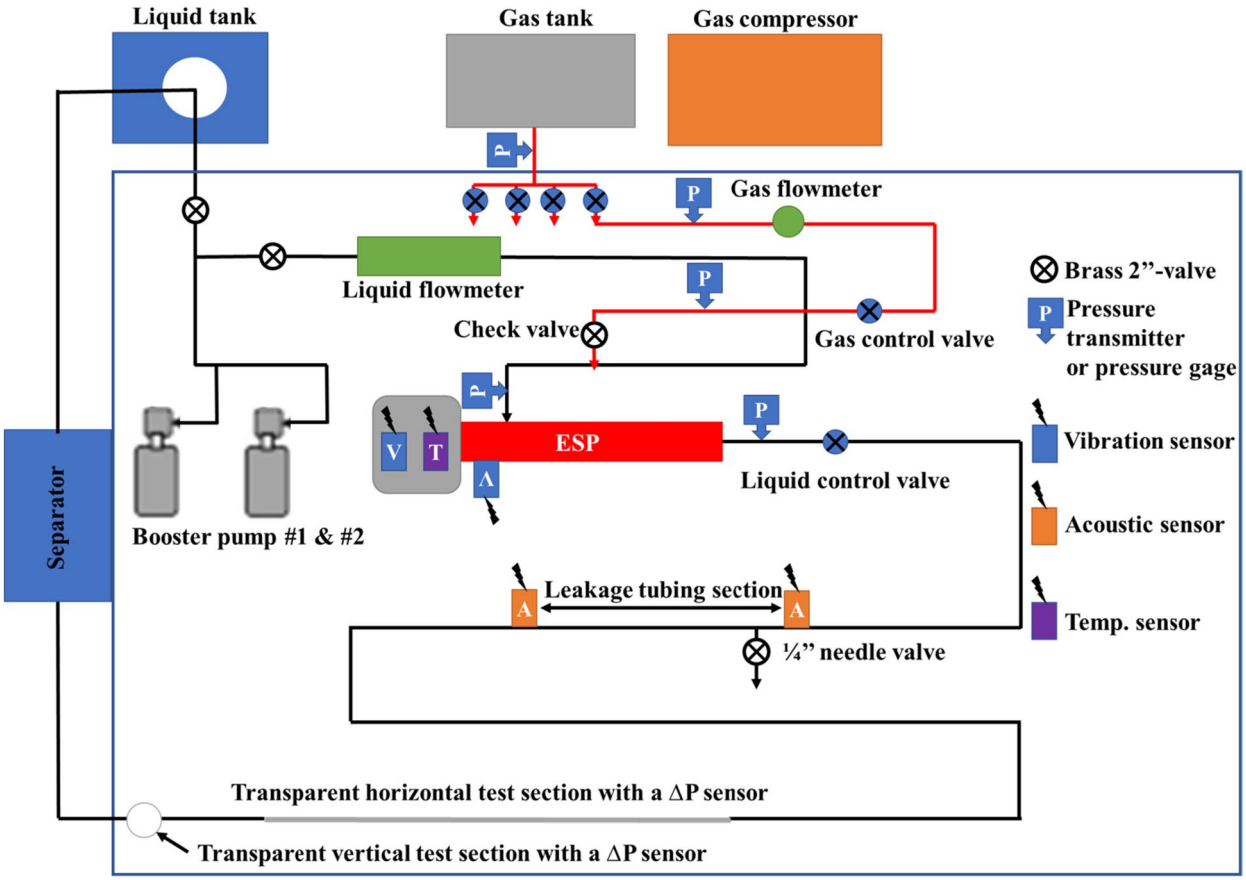

Fig. 3 Schematic diagram of the experimental system

Fresh water and air were used as testing fluids. The controllable variables were the pump speeds, water–gas ratios, pump intake and discharge pressures. The data acquisition system recorded the pump performance in both the single- and multi-phase flow conditions.

The water from the liquid tank flowed into the pipes connected to the pump intake. The water rate was measured by the liquid flow meter. The gas was controlled using the valves and is injected into the pipeline before the pump intake. The gas rate was controlled using the valves and is measured using the gas flowmeter. Further, a pressure gage was installed at the pump in/out section to measure the pressure. The water and the injected gas were pumped through the leakage tubing section equipped with two acoustic sensors. The injected fluid flowed through the transparent sections and reached the gas/liquid separator, where the liquid and gas phases were separated to allow only the water to flow back into the liquid tank.

The sensors installed in the ESP experimental system were two vibration sensors, two acoustic sensors, one temperature sensor and seven pressure sensors. During the pump performance tests, one vibration sensor was installed on the motor and the other sensor was attached to the inlet of the pump. However, the sensor at the pump inlet malfunctioned. As a result, the signal was not of good quality and was excluded from the analysis. Therefore, 11 variables of raw data, including the liquid rate, intake/discharge pressures, the pressure difference of horizontal and vertical test, the pressure of the separator, the liquid level of the separator, temperature of the motor and winding, the vibration of the motor, and acoustic amplitude, were continuously measured during the test. The data analyzed in this study was obtained for 300 days from April 8, 2021, to February 2, 2022.

Analysis of the experimental results

The signals of all the variables obtained during the ESP test are shown in Figs. 4, 5, 6, 7 and 8. In this study, the ESP failure was defined through the irrecoverable and uncontrollable ESP performance drop during operation. There were two failures during the 300-day experiment: on days 112 and 271. The first failure, on day 112, was induced by the excessive friction due to a lack of lubricant. The test was restarted from day 139, after 27 days of maintenance, without any replacements to ensure consistency during experimentation. The second failure occurred on day 271, and the test was terminated at day 300. The performance of the ESP can be observed in the liquid rate, intake pressure and discharge pressure, as indicated by the blue, red, and green curves, respectively, in Fig. 4. The liquid rate and pressure behaviors at the first and second failures were magnified, as shown in Fig. 4b and c, respectively. Before the first failure, the liquid rate, intake pressure, and discharge pressure were, in average, 86.02 m^3/day, 27.43 kPa, and 4.04 MPa, respectively. However, after the first failure on day 112, the performance of the ESP dropped drastically, and the liquid rate and pressures dropped to 3.86 m^3/day, 25.04 kPa, and 2.81 MPa, respectively (Fig. 4b). After the maintenance on day 139, the liquid rate was stabilized at 105.78 m^3/day. Although the maintenance was completed, the performance did not

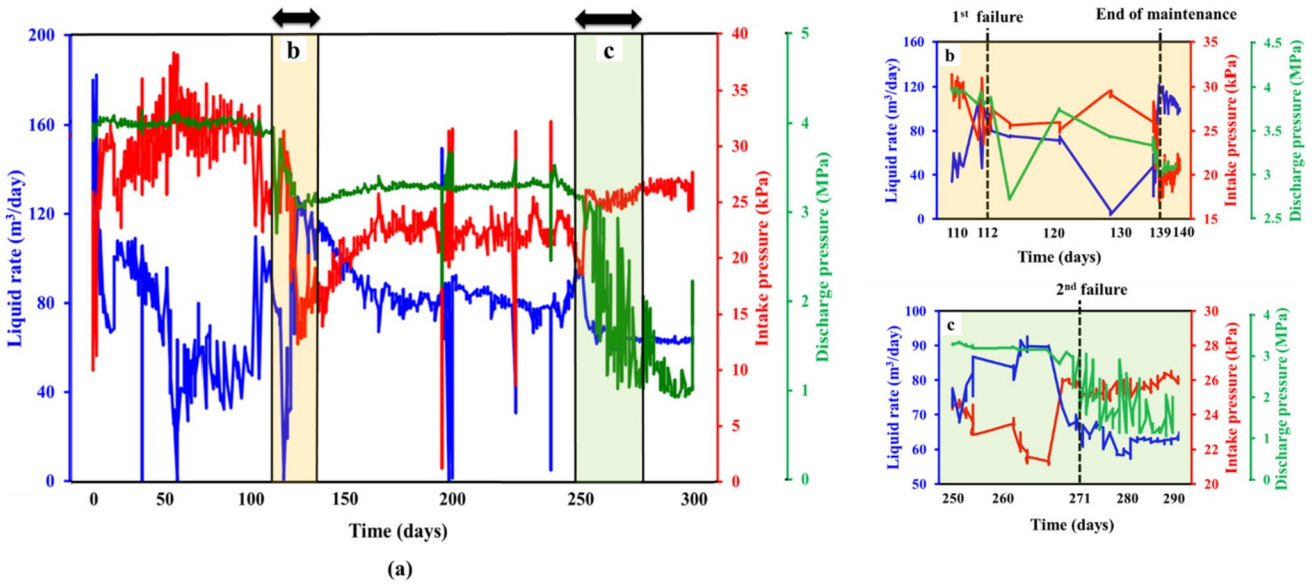

Fig. 4 **a** Measured data of the liquid rate, intake pressure, and discharge pressure during the 300-day experiment. The signals during **b** the first and **c** second failures are magnified

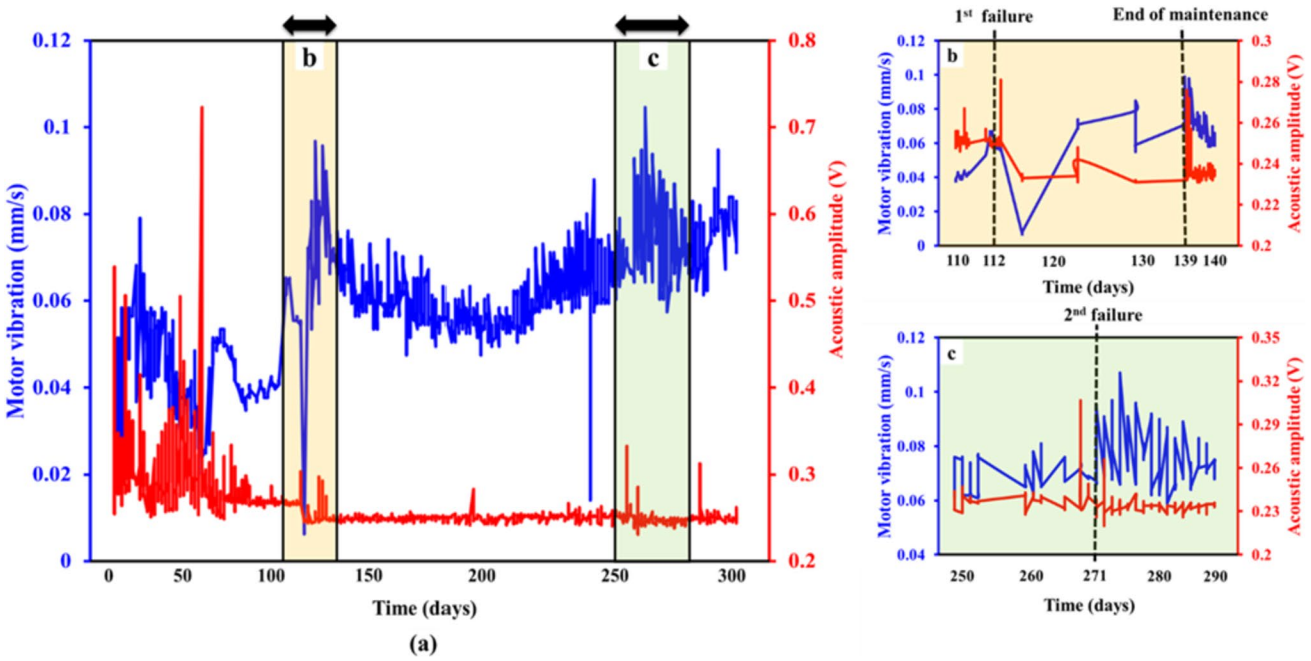

Fig. 5 **a** Measured data of the motor vibration and acoustic amplitude during the 300-day experiment. The signals during **b** the first and **c** second failures are magnified

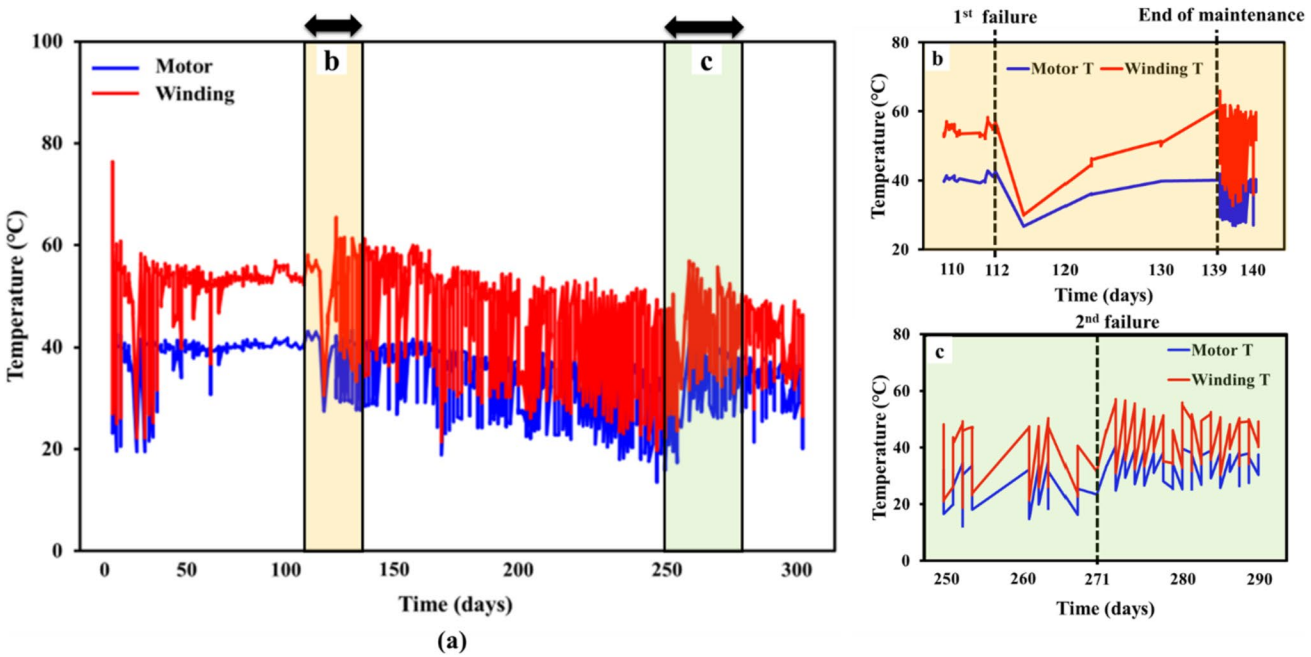

Fig. 6 **a** Measured data of the motor and winding temperature during the 300-day experiment. The signals during **b** the first and **c** second failures are magnified

recover to its original values, as the average rate and pressures were 82.87 m^3/day, 23.28 kPa, and 3.29 MPa, respectively. At the second failure in Fig. 4c, the liquid rate and the discharge pressure dropped from 92.63 m^3/day and 3.39 MPa to 57.33 m^3/day and 1.11 MPa, respectively. In addition, the intake pressure was increased from 21.46 kPa to 25.89 kPa. The liquid rate, intake pressure,

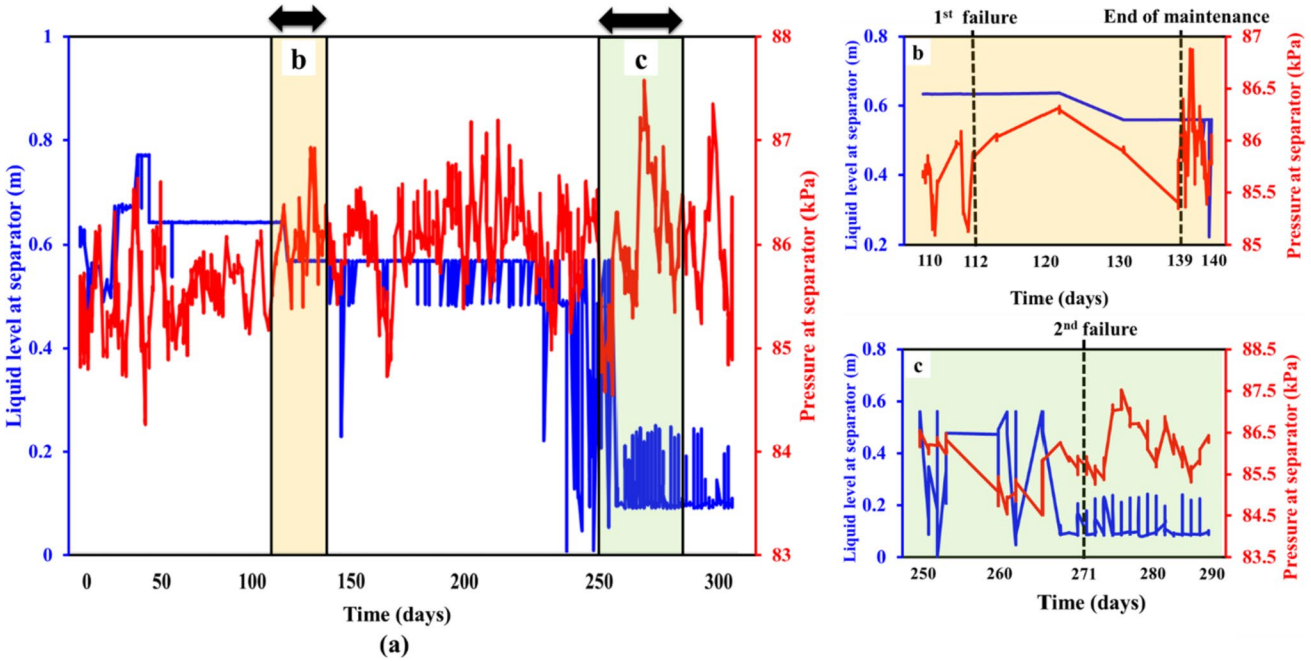

Fig. 7 **a** Measured data of the liquid level and pressure at the separator during the 300-day experiment. The signals during **b** the first and **c** second failures are magnified

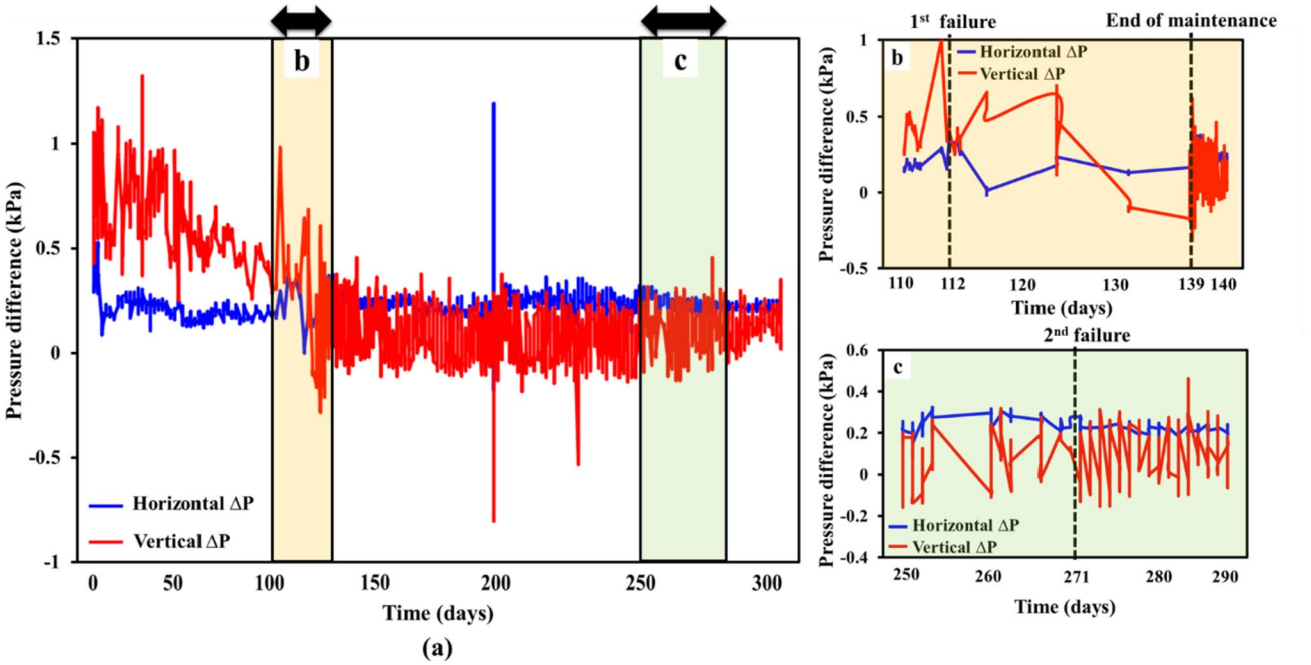

Fig. 8 **a** Measured data of the horizontal and vertical pressure differences during the 300-day experiment. The signals during **b** the first and **c** second failures are magnified

and discharge pressure never recovered to attain their initial states.

The blue and red curves in Fig. 5 show the motor vibration and acoustic amplitude, respectively. Before the first failure, the motor vibration and acoustic amplitude were, in average, 0.02–0.08 mm/s and 0.26 V, respectively. After the first failure on day 112, the motor vibration and acoustic amplitude decreased to 0.01 mm/s and 0.24 V, respectively

(Fig. 5b). Additionally, after the maintenance on day 139, the average motor vibration and acoustic amplitude were stabilized at 0.07 mm/s and 0.24 V, respectively. Despite the maintenance was conducted, the average values of the signals did not recover to their values before the failure. In average, the motor vibration range and acoustic amplitude were 0.05–0.09 mm/s and 0.24 V, respectively. At the second failure in Fig. 5c, the motor vibration increased in the range of 0.06–0.11 mm/s, which was an increase from the previous range. Also, the acoustic amplitude increased to 0.31 V just before the second failure and then stabilized at 0.23 V in average.

The temperatures of the motor and winding are depicted through the blue and red curves, respectively, in Fig. 6. Before the first failure, the motor and winding temperatures were 39.52 °C and 53.77 °C, respectively, in average, and then decreased to 37.72 °C and 52.82 °C, respectively, in average, after the first failure (Fig. 6b). Additionally, the motor and winding temperatures dropped to 30.74 °C and 42.06 °C, respectively, in average, after the maintenance on day 139. At the second failure in Fig. 6c, the motor temperature was slightly increased to 31.01 °C in average, and the winding temperature was marginally decreased to 41.51 °C in average.

The blue and red curves in Fig. 7 shows the liquid level and pressure, respectively, at the separator. The liquid level at the separator was in the range of 0.48–0.76 m at the beginning of the experiment, and then stabilized at 0.63 m. The pressure at the separator was 85.36 kPa in average before the first failure. After the first failure, the liquid level decreased to 0.56 m, and the pressure at the separator stabilized at 85.37 kPa (Fig. 7b). Furthermore, after the maintenance on day 139, as shown in Fig. 7b, the liquid level was at an average of 0.56 m, and the pressure was observed to be 85.99 kPa in average. At the second failure in Fig. 7c, the liquid level sharply decreased to 0.09 m in average, and the pressure at the separator was observed to be 86.05 kPa in average.

The horizontal and vertical pressure differences were monitored at the transparent sections, as shown in Fig. 3, and are represented by the blue and red curves, respectively, in Fig. 8. Before the first failure, the horizontal pressure difference stabilized at 0.23 kPa, and the vertical pressure difference showed a decreasing trend, with an average of 0.68 kPa. Although the first failure occurred, the horizontal pressure difference slightly decreased to 0.22 kPa in average while the vertical pressure difference significantly decreased to −0.19 kPa in average (Fig. 8b). After the maintenance on day 139, the horizontal pressure difference still stabilized at 0.22 kPa, and the vertical pressure difference considerably increased to 0.08 kPa. At the second failure in Fig. 8c, the horizontal and vertical pressure differences were stabilized at 0.22 kPa and 0.08 kPa in average, respectively.

Consequently, to identify and diagnose the ESP failure and its performance drop is a complicated process, especially in real-time. In addition, it is challenging to interpret and integrate the parameters that might contain information, due to its various behaviors in largely diversified ranges. Therefore, in this study, PCA was adopted for reliable analysis of the ESP failure and performance.

Application of PCA

Although the measured parameters contain useful information about the ESP performance, it is challenging to integrate these due to their various behavior and ranges. PCA is a widely used unsupervised machine learning method that reduces the dimensions of original data and generates a new set of principal components for more reliable data analysis and visualization (Raschka and Raschka 2014; Oliveira et al. 2021). To develop a PCA model, the interdependencies in the target data are used with the dimensionality reduction of all the data variables (Jolliffe and Cadima 2016). Generally, ESP data are highly correlated. For example, an increase in the wellhead pressure causes an increase in the discharge pressure, which finally leads to an increase in the motor temperature (Peng et al. 2020). Therefore, in this study, the PCA method was adopted for the ESP failure diagnosis and performance analysis with the principal component. Based on Eriksson et al. (2013), the basic PCA model is represented as follows:

$$X = TP^T + E \tag{1}$$

where X is the input matrix ($t \times p$); T is the score matrix ($t \times N$); P is the loading matrix ($p \times N$); E is the residual matrix ($t \times p$); t is the number of time steps; p is the number of original parameters; and N is the number of principal components. The first principal component contains the most information of all the data, as it captures the highest possible variance. The second principal component captures the second highest variance. With this principle, the third, fourth, and Nth component can be created to evaluate the entire ESP system. Each component will be orthogonal to its preceding components, which led to the PCs captured by the PCA model being irrelevant to each other (Hua et al. 2007). This results in the dimensionality reduction of the target variables by taking advantage of the linear combinations and by creating new PCs (Abdi and Williams 2010). These PCs can evaluate the ESP system only by several PCs, making the process much easier. This way, the PCA method eliminates all dependencies within the principal components and captures the relevant information.

In this study, a PCA model was constructed to reduce the dimensionality of the normal status data including the

11 parameters, and extract the PCs that capture most of the information in the normal status data. In addition, we aimed to visually analyze the PCA model by training the strong patterns in the normal status data and evaluating the model with the testing data including both the normal and failure status. In short, the experimental period was divided into the normal and failure status. The periods with the normal status were before the first failure on day 112 and between the maintenance completed on day 139. The second failure on day 271. Otherwise, the periods were defined as the failure status. The PCA model was constructed with the 8,928 data points obtained from the normal status. The loading matrix for the normal status data was stored to enable prediction at the testing stage. Once the PCA model was ready, a new input dataset was chosen as the testing data, and 1,027 data points were obtained between the days 238 and 300 during both the normal and failure status. The testing data was fed into the developed PCA model as a new score matrix. The patterns of the testing data were compared with the patterns trained by the PCA model to make predictions. Consequently, the data obtained from the ESP testing system was identified by the developed PCA model.

Data analysis and normalization

In this study, it was assumed that information about the ESP performance and its failure was contained in the 11 measured parameters, i.e., liquid rate, pressures of the pump

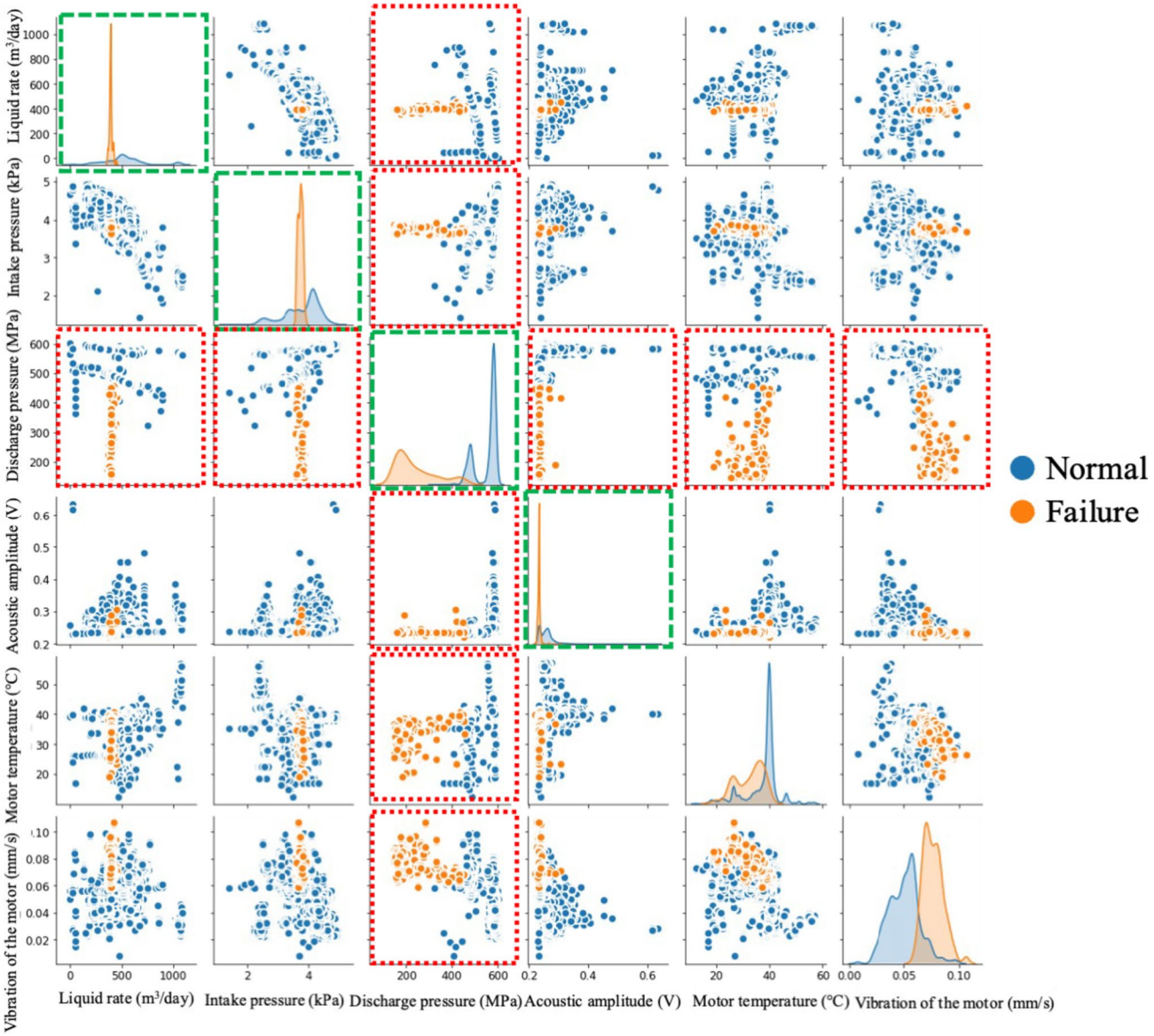

Fig. 9 Example of pairplot for the liquid rate, intake pressure, discharge pressure, acoustic amplitude, motor temperature, and motor vibration

intake and discharge, separator pressure, liquid level in the separator, horizontal and vertical difference pressures, motor vibration, acoustic amplitude, and the temperatures of the motor and winding. The 9,955 data points achieved from the normal and failure status were analyzed to identify the representative patterns for each status. Figure 9 shows the example of a pairplot for the liquid rate, intake pressure, discharge pressure, acoustic amplitude, the motor temperature, and the motor vibration data during the normal and failure status. The pairplot is a useful visualization tool that examines the pairwise relationships between different variables (Thakur and Samuel 2021). Through a pairplot, the normal and failure status can be clearly distinguished by the histograms of the liquid rate, intake pressure, discharge pressure, and acoustic amplitude (green-dashed rectangles in Fig. 9). In addition, the normal and failure status can be differentiated if the relationships between the discharge pressure, liquid rate, acoustic amplitude, motor temperature and motor vibration are investigated (red-dotted rectangles in Fig. 9). However, since it can be seen that the signals for both the normal and failure status were mixed, there was, visually, no clear trend or characteristic to identify the status in other plots. Furthermore, it indicated that there was a relationship between the liquid rate and intake pressure, and discharge pressure and the vibration of the motor. Since there was a limitation for visually analyzing the relationship, the Pearson correlation method was adopted to quantitively identify and analyze the relationship and dependency between the parameters. The Pearson correlation method is widely used to understand the correlation between various variables and to improve the effectiveness of a PCA method (Wang et al. 2022). With this method, a PCA method can achieve by minimizing the number of variables while retaining more information to ensure that the analysis is not going to be affected after applying a PCA method when there are a large number of linearly correlated variables in the multi-parameters (Teng et al. 2017). The Pearson correlation coefficient, r_{xy}, can be determined by,

$$r_{xy} = \frac{\sqrt{x_i y_i} - n\overline{xy}}{\sqrt{\left(\sum x_i^2 - n\overline{x^2}\right)}\sqrt{\left(\sum y_i^2 - n\overline{y^2}\right)}} \tag{2}$$

where, n is the sample size, x_i and y_i are the individual sample points indexed with $\overline{x}$ and $\overline{y}$ are the mean values of the target parameters x and y, respectively. The Pearson correlation coefficient r_{xy} is a value between -1 and 1. The value of -1, 0, and 1 indicate perfectly negative correlation, no correlation, and perfectly positive correlation, respectively. In addition, the correlation levels are defined as 0.00–0.25 (very weak), 0.26–0.49 (weak), 0.50–0.69 (moderate), 0.70–0.89 (strong), and 0.90–1.0 (very strong) (Rienstra et al. 2015). The calculated Pearson correlation coefficients between the input parameters are shown in Fig. 10. The coefficients were distributed within the range from -0.77 to 0.98. It can be seen from the Fig. 10 that the motor temperature had a very strong correlation level with the winding temperature ($r_{xy} = 0.98$). The intake pressure also showed a strong correlation level with the liquid rate ($r_{xy} = -0.77$) and horizontal pressure difference ($r_{xy} = -0.77$), between the liquid rate and horizontal pressure difference ($r_{xy} = 0.85$). The discharge pressure had a strong correlation level with the separator liquid level ($r_{xy} = 0.79$). Also, there were variables indicating the correlation level of moderate. For example, between the discharge pressure and vertical pressure difference ($r_{xy} = 0.60$); the discharge pressure and the motor vibration ($r_{xy} = -0.62$); vertical pressure difference and motor vibration ($r_{xy} = -0.59$); and the separator liquid level and motor vibration ($r_{xy} = -0.53$). Moreover, there were 46 relationships with correlation levels of weak and very weak. Therefore, although the dependencies between the measured parameters were diversified, there are variables with strong and very strong correlation levels, which makes it reliable to adopt the PCA method for the dimensionality reduction. When the representative characteristics were extracted from the data of the ESP testing system, the PCA method would be effective for failure diagnosis.

Meanwhile, diversity in the data range obtained during the ESP experiment needs to be taken into account. In the PCA model, the obtained data were scaled by the Robust scaler in the Scikit-learn package. The Robust scaler uses an interquartile range; it is thus robust to outliers (Keen 2018) and calculates the scaling value for each feature as follows,

$$S = \frac{x - Q1(x)}{Q3(x) - Q1(x)} \tag{3}$$

where x is the input value; S is the scaling factor; and Q is the interquartile range of x.

PCA model construction

The PCA model, constructed with the 11 measured parameters to reduce the dimensionality of the 8,928 pieces of normal status data, aimed at identifying the patterns for the normal and failure status with the extracted PCs. There were three PCs, each of which captured 88.3% of the data variance. Each PC, i.e., PC 1, PC 2 and PC 3, captured 54.7%, 20.6%, and 13.0% of the data variance, respectively (Fig. 11). According to Géron (2019), PCs capturing 80.0% or higher of data variance show representativeness. Consequently, it was concluded that the three PCs represented the measured experimental data sufficiently.

Figure 12a and b show examples of the measured parameters and the three extracted PCs from days 45 to 55. Although the 11 parameters obtained for the experiment

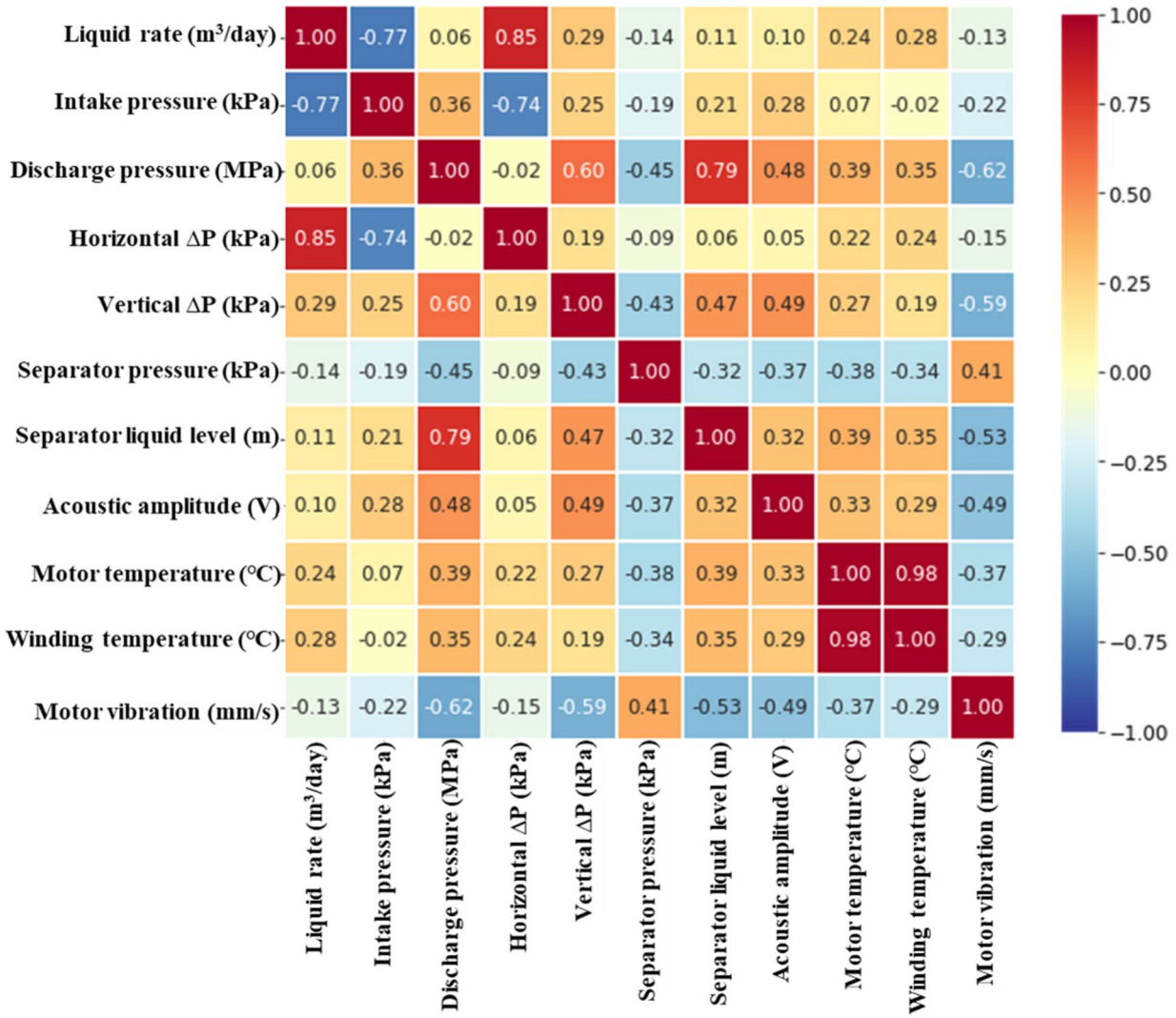

Fig. 10 The Pearson correlation heatmap for the input parameters

were normalized, the behaviors were diversified, and no clear trend was observed (Fig. 12a). The representative characteristics of the measured parameters were captured by the three PCs, as shown in Fig. 12b. Each PC contained a different percentage of the total variance, and the PC 1 showed a larger representativeness. Only the three PCs were used to evaluate the ESP performance and diagnose ESP failure. Consequently, it was found that the developed PCA model provided an intuitive way to analyze and diagnose the ESP performance.

PCA model testing and results

The PCA model testing was performed with the 1,027 data points obtained from both the normal and failure status. The testing results were analyzed with the three PCs to assess the applicability of the PCA model. The two- and three-dimensional score plots for training and testing the model were visualized to identify the ESP failure diagnosis and undertake performance analysis (Fig. 13). The blue-, green-, and yellow-dotted rectangles indicate the planes with the PC 1, 2, and 3 equal to 0, respectively. In addition, the planes corresponded to the dotted lines with the same colors in the two-dimensional plots, as shown in Fig. 13. Figure 13a and b depict the three-dimensional score plots for training and testing the PCA model. The blue and red dots indicate the normal and failure status, respectively.

The two-dimensional score plots between the PCs, as shown in Fig. 13c and d, were used to analyze the efficiency of each PC for ESP failure diagnosis. When tested with the data obtained from both the normal and failure status, PC 1 was always greater than 0. However, it was hard to distinguish between the normal and failure status with PC 1. On the other hand, when PC 1 and PC 2 were considered,

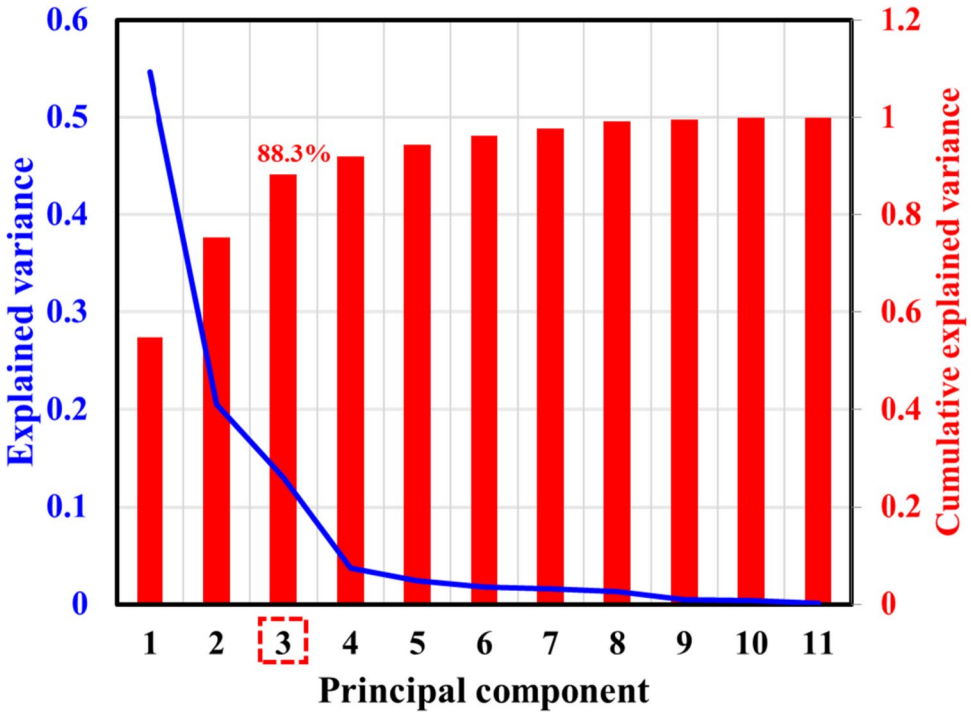

Fig. 11 Explained variance for each principal component and cumulative explained variance

PC 2 had values lower than 3.21 and higher than 4.41 for the normal and failure status, respectively. Meanwhile, there was a transition zone between 3.21 and 4.41, where both the normal and failure status existed. In the same manner, when PC 3 was investigated in terms of PC 1 and PC 2, the normal status was observed when PC 3 was higher than −0.89, and higher −0.81, respectively (Fig. 13d). Moreover, the failure status was also spotted by the PC 3 values, as it was lower than −3.08 for both PC 1 and PC 2. Therefore, the developed PCA model allowed the distribution of the PCs to visually distinguish between the normal and failure status, and to establish criteria to identify normal, failure, and transition zone.

A confusion matrix was used to analyze the performance of the developed PCA model, evaluate the reliability of the prediction results, and address the potential errors. There were four possible binary classification outcomes in a confusion matrix (Andrade Marin et al. 2019). To generate the prediction results, the logistic regression method in the Scikit-learn package was adopted with all of the 11 variables and three PCs. A total of 8,928 data points from the normal status were used to train the model, and 490 and 537 data points from the normal and failure status, respectively, were used to tested the model. Figure 14 summarizes the matrix results in the confusion matrix. As shown in Fig. 14, when the measured data were considered, the prediction accuracy of the normal status was 100.0%, and 51 failure data points were not accurately identified. On the contrary, using the extracted three PCs, 501 true failure status of the 537 failure status data were predicted by the PCA model with improved accuracy. Since the three PCs represented 88.3% of the 11 variables of ESP performance, the remaining 11.7% was neglected and 37 data points (36 failure and 1 normal status) were not accurately diagnosed (Fig. 11).

Discussion

In this study, the PCA method was adopted to diagnose ESP failure. To achieve more realistic data, an experiment was performed for 300 days, with an experimental system constructed particularly for the study. The extended period of the experiment proved effective in terms of enhancing the quality of the analysis. Defining the ESP failure as an uncontrollable drop in performance, two failures were observed, on days 112 and 271, during the experiment period.

Based on the measured data, three PCs were extracted to represent the trends of the normal and failure status. It was found that the three PCs captured 88.3% of the characteristics of the measured data. Although the three PCs contained 88.3% of the information, 11.7% of the information was missing. As a result, the status of the ESP was not accurately diagnosed from the 36 data points measured during the failure status. In this manner, since the PCA method performed with dimensionality reduction of high-dimensional data, there was a likelihood of useful information being missed. In addition, data normalization was essential before performing the method because the PCA method is sensitive to outliers (Sapra 2010). Although the PCA method has limitations, it has been adopted in various fields because it is useful

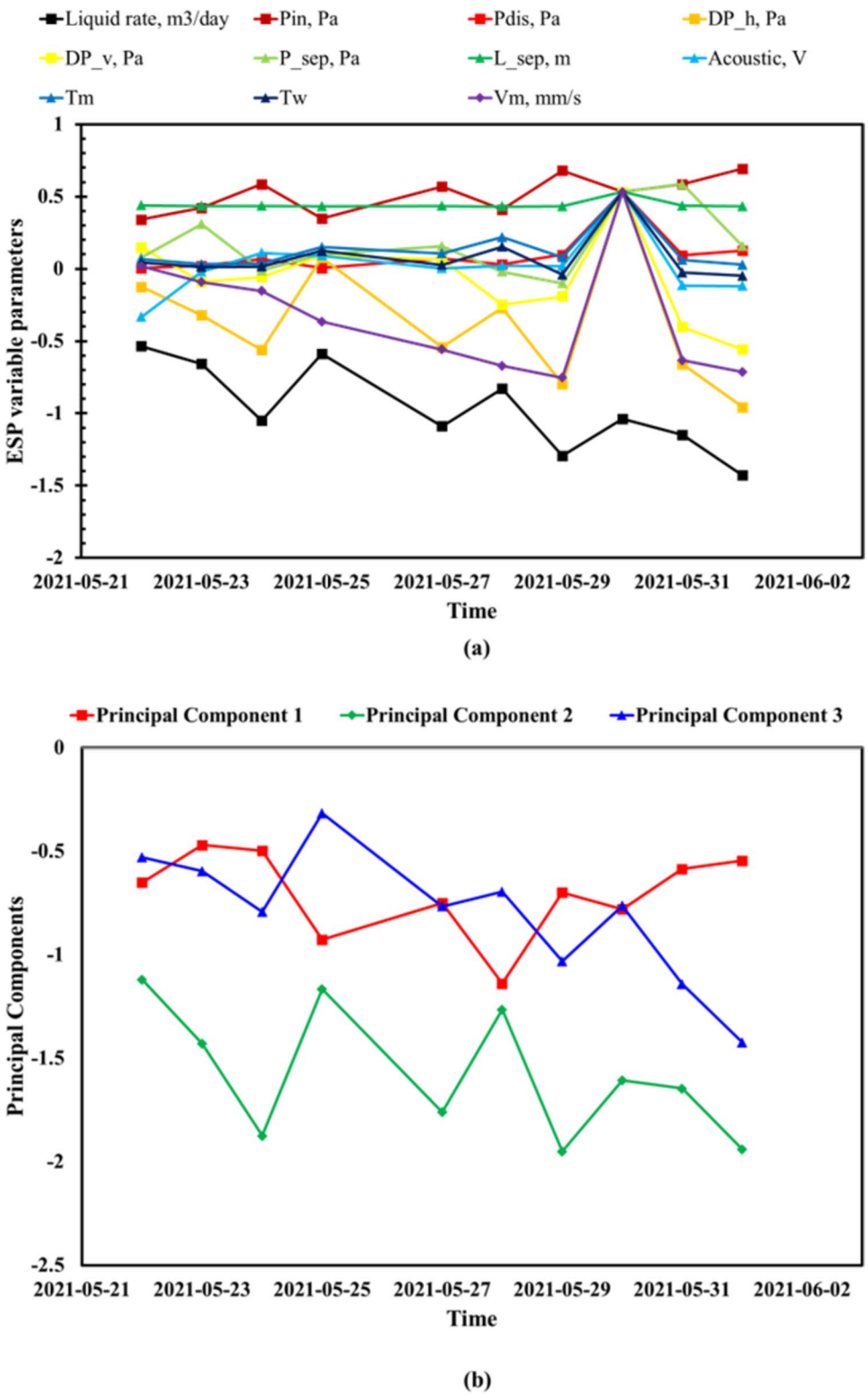

Fig. 12 Examples of **a** plots of the normalized normal status data from 11 variables and **b** plots for the extracted new three PCs during days 45–55

for data analysis and visualization through dimensionality reduction, and its applicability has been verified (Gottumukkal and Asari 2004; Salo et al. 2019; Singh et al. 2022). Therefore, one of the aims of the future study is to focus on how to improve the representativeness of the PCs and to enhance the accuracy of the failure diagnosis.

There are various causes of ESP failure, such as centrifugal pump failure, cable failure, motor failure, and

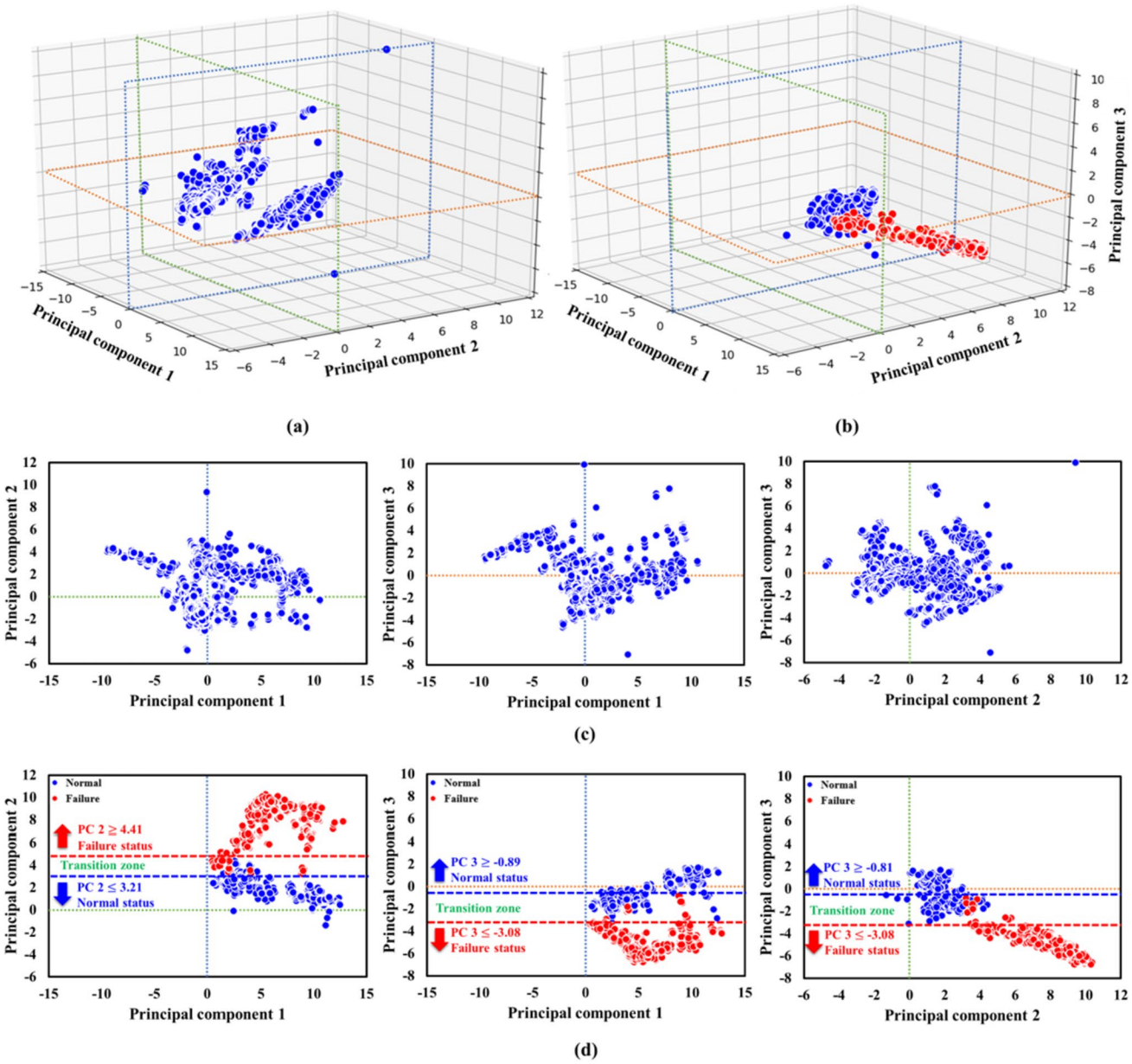

Fig. 13 Three-dimensional score plots of the three PCs for **a** the training and **b** testing results of the PCA model. Also, the two-dimensional score plots of the two PCs for **c** the training and **d** testing results

unbalanced motor three-phase direct resistance, etc. (Alhanati et al. 2001). If the PCA model is developed after obtaining data on each cause of failure by continuously performing the ESP experiment, the integrated failure diagnosis of the ESP can be performed. Furthermore, this integrated ESP failure diagnostic PCA model can be put to practical use in the field, which is considered to be robust tool for designing production strategies.

Conclusions

In this study, the principal component analysis (PCA) method was adopted for electrical submersible pump (ESP) failure diagnosis and its performance analysis based on the data measured from the ESP experimental system. Based on the primary observations, the following conclusions can be drawn.

1. The ESP experimental system comprised a 20 stage ESP, a 50 hp 480 V motor, a gas–liquid separator, a liquid

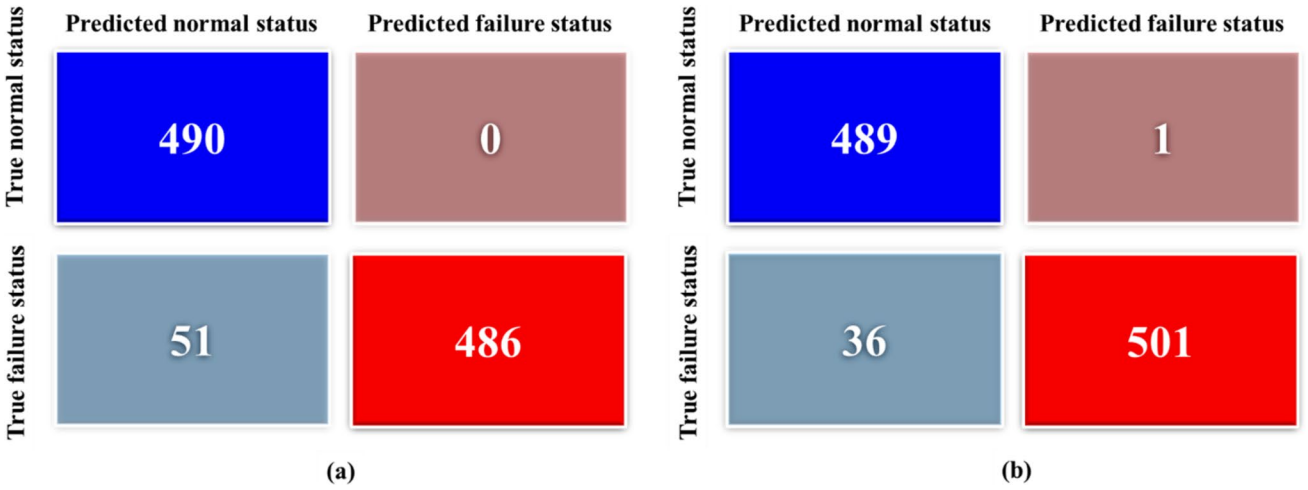

Fig. 14 Comparison of confusion matrix of ESP failure analysis using **a** original data with 11 parameters and **b** three PCs

tank, gas and liquid flow meters, gas and liquid control valves, pressure and temperature sensors and a transmitter. The experiment was performed for 300 days, and 11 variables were measured.

2. The ESP failure was defined by an uncontrollable drop in performance during operation. There were two failures during the 300-day experiment: on days 112 and 271. It was found that all the measured parameters started to behave abnormally as soon as the ESP failed. In addition, it was found that the ESP performance drop did not recover its original value after the failure.
3. A PCA model was constructed with 8,928 normal status data and tested with the 1,027 normal and failure status data. According to the two- and three-dimensional analyses, the ESP failure can be diagnosed visually with the developed PCA model. In addition, the PCA model provided an intuitive way to distinguish between normal and failure status and establish criteria to identify the normal, failure, and transition zones.
4. To investigate the efficiency of the PCA model, both the 11 variables and the three principal components were compared by the confusion matrix using the logistic regression method. The results showed that the developed PCA model can be used to diagnose the status of the ESP with better accuracy of 93.3%.

Therefore, it can be concluded that PCA is an effective method for ESP failure diagnosis and undertaking performance analysis. Moreover, the PCA method is also an efficient dimensionality reduction method for the ESP failure diagnosis by integrating data analysis.

Funding This work is supported by the Korea Institute of Energy Technology Evaluation and Planning (KETEP) grant funded by the Korean Government Ministry of Trade, Industry & Energy (No. 20216110100010 and No. 20214710100060).

Declarations

Conflict of interest The authors have no relevant financial or non-financial interests to disclose.

References

Abdelaziz M, Lastra R, Xiao JJ (2017) ESP data analytics: predicting failures for improved production performance. In: Abu Dhabi international petroleum exhibition & conference. https://doi.org/10.2118/188513-MS

Abdi H, Williams LJ (2010) Principal component analysis. Wiley Interdiscip Rev Comput Stat 2:433–459. https://doi.org/10.1002/wics.101

Alamu OA, Pandya DA, Warner O, Debacker I (2020) ESP data analytics: use of deep autoencoders for intelligent surveillance of electric submersible pumps. In: Offshore technology conference. OnePetro. https://doi.org/10.4043/30468-MS

Alhanati FJS, Solanki SC, Zahacy TA (2001) ESP failures: can we talk the same language? In: SPE Gulf Coast section electric submersible pump workshop. OnePetro. https://doi.org/10.2118/148333-MS

Al-Janabi MAM, Al-Fatlawi O (2022) Gas lift optimization: a review. In: AIP conference proceedings. AIP Publishing LLC, p 30013. https://doi.org/10.1063/5.0091901

AlJuboori M, Hossain M, Al-Fatlawi O, et al (2020) Numerical simulation of gas lift optimization using genetic algorithm for a Middle East oil field: feasibility study. In: International petroleum technology conference. OnePetro. https://doi.org/10.2523/IPTC-20254-MS

Andrade Marin A, Busaidy S, Murad M, et al (2019) ESP well and component failure prediction in advance using engineered analytics-a breakthrough in minimizing unscheduled subsurface deferments. In: Abu Dhabi international petroleum exhibition & conference. OnePetro. https://doi.org/10.2118/197806-MS

Asadi S, Rao C, Saikrishna V (2010) A comparative study of face recognition with principal component analysis and cross-correlation technique. Int J Comput Appl 10:17–21. https://doi.org/10.5120/1502-2019

Awaid A, Al-Muqbali H, Al-Bimani A, et al (2014) ESP well surveillance using pattern recognition analysis, oil wells, petroleum development Oman. In: IPTC 2014: international petroleum technology conference. European Association of Geoscientists & Engineers, p cp-395–00213. https://doi.org/10.2523/IPTC-17413-MS

Ballarini M, Bruni M, Muñoz H, et al (2017) High efficiency ESP applications for slim wells. In: SPE electric submersible pump symposium. OnePetro. https://doi.org/10.2118/185137-MS

Bates R, Cosad C, Fielder L et al (2004) Taking the pulse of producing wells—ESP surveillance. Oilf Rev 16(2):16–25

Carobene A, Campagner A, Uccheddu C et al (2022) The multicenter European Biological Variation Study (EuBIVAS): a new glance provided by the principal component analysis (PCA), a machine learning unsupervised algorithms, based on the basic metabolic panel linked measurands. Clin Chem Lab Med 60:556–568. https://doi.org/10.1515/cclm-2021-0599

Carrillo W (2013) Prognostics for oil & gas artificial lift applications. New Orleans GE Oil Gas

Chu T, Nguyen TC, Wang J et al (2021) New correlations for predicting two-phase electrical submersible pump performance under downhole conditions using field data. J Petrol Explor Prod Technol 12:1225–1235. https://doi.org/10.1007/s13202-021-01392-y

Dunham C (2013) 27th ESP Workshop: summary of presentations. Artificial Lift R&D Council, April 2013. Oilf Autom Consult 1: https://www.spegcs.org/media/files/files/cebfcc3a/2013-ESP-Workshop-Summary-of-Presentations.pdf.

Eriksson L, Byrne T, Johansson E, et al (2013) Multi-and megavariate data analysis basic principles and applications. vol. 1, Umetrics Academy

Fakher S, Khlaifat A, Hossain ME, Nameer H (2021) Rigorous review of electrical submersible pump failure mechanisms and their mitigation measures. J Pet Explor Prod Technol 11:3799–3814. https://doi.org/10.1007/s13202-021-01271-6

Géron A (2019) Hands-on machine learning with Scikit-Learn, Keras, and TensorFlow: concepts, tools, and techniques to build intelligent systems. O'Reilly Media, Inc.

Gottumukkal R, Asari VK (2004) An improved face recognition technique based on modular PCA approach. Pattern Recognit Lett 25:429–436. https://doi.org/10.1016/j.patrec.2003.11.005

Guindi R, Storts B, Beard J (2017) Case study, permanent magnet motor operation below perforations in stagnant fluid. In: SPE electric submersible pump symposium. OnePetro. https://doi.org/10.2118/185273-MS

Guo D, Raghavendra CS, Yao K-T, et al (2015) Data driven approach to failure prediction for electrical submersible pump systems. In: SPE western regional meeting. https://doi.org/10.2118/174062-MS

Gupta S, Nikolaou M, Saputelli L, Bravo C (2016a) ESP health monitoring KPI: a real-time predictive analytics application. In: SPE intelligent energy international conference and exhibition. https://doi.org/10.2118/181009-MS

Gupta S, Saputelli L, Nikolaou M (2016b) Applying big data analytics to detect, diagnose, and prevent impending failures in electric submersible pumps. In: SPE annual technical conference and exhibition. https://doi.org/10.2118/181510-MS

Gupta S, Saputelli L, Nikolaou M (2016c) Big data analytics workflow to safeguard ESP operations in real-time. In: SPE North America artificial lift conference and exhibition. OnePetro. https://doi.org/10.2118/181224-MS

Hamzah K, Prakoso NF, Dwitiya D, et al (2017) Extensive application of ESP with permanent magnet motor: continuous improvement for energy saving and cost reduction. In: SPE symposium: production enhancement and cost optimisation. OnePetro. https://doi.org/10.2118/189211-MS

Hua XG, Ni YQ, Ko JM, Wong KY (2007) Modeling of temperature–frequency correlation using combined principal component analysis and support vector regression technique. J Comput Civ Eng 21:122–135. https://doi.org/10.1061/(ASCE)0887-3801(2007)21:2(122)

Insuasty E, Van den Hof PM, Weiland S, Jansen JD (2017) Low-dimensional tensor representations for the estimation of petrophysical reservoir parameters. In: SPE reservoir simulation conference. OnePetro. https://doi.org/10.2118/182707-MS

Jolliffe IT, Cadima J (2016) Principal component analysis: a review and recent developments. Philos Trans R Soc A Math Phys Eng Sci 374:20150202. https://doi.org/10.1098/rsta.2015.0202

Keen BA (2018) Feature scaling with scikit-learn. http://benalexkeen.com/feature-scaling-with-scikit-learn/. Accessed 16 May 2023

Kolawole O, Gamadi T, Bullard D (2019) Comprehensive review of artificial lift system applications in tight formations. SPE East. Reg. Meet. D021S002R008. https://doi.org/10.2118/196592-MS

Li C, Diao Y, Ma H, Li Y (2008) A statistical PCA method for face recognition. In: 2008 Second international symposium on intelligent information technology application. IEEE, pp 376–380. https://doi.org/10.1109/IITA.2008.71

Nguyen T (2020) Artificial lift methods: design, practices, and applications. Springer Nature

Oliveira BCF, Seibert AA, Borges VK et al (2021) Employing a U-net convolutional neural network for segmenting impact damages in optical lock-in thermography images of CFRP plates. Nondestruct Test Eval 36:440–458. https://doi.org/10.1080/10589759.2020.1758099

Peng L, Han G, Landjobo Pagou A, Shu J (2020) Electric submersible pump broken shaft fault diagnosis based on principal component analysis. J Pet Sci Eng 191:107154. https://doi.org/10.1016/j.petrol.2020.107154

Peng L, Han G, Sui X et al (2021) Predictive approach to perform fault detection in electrical submersible pump systems. ACS Omega 6:8104–8111. https://doi.org/10.1021/acsomega.0c05808

Phillips PJ, Flynn PJ, Scruggs T, et al (2005) Overview of the face recognition grand challenge. In: 2005 IEEE computer society conference on computer vision and pattern recognition (CVPR'05). IEEE, pp 947–954. https://doi.org/10.1109/CVPR.2005.268

Raschka S, RASCHKA S (2014) Predictive Modeling, supervised machine learning, and pattern classification-the big picture. Sebastian Raschka

Ratcliff DE, Gomez C, Cetkovic I, Madogwe O (2013) Maximizing oil production and increasing ESP run life in a brownfield using real-time ESP monitoring and optimization software: rockies field

case study. In: SPE annual technical conference and exhibition. OnePetro. https://doi.org/10.2118/166386-MS

Refai A, Abdou HAM, Seleim A, et al (2013) Permanent magnet motor application for ESP artificial lift. In: North Africa technical conference and exhibition. OnePetro. https://doi.org/10.2118/164666-MS

Rienstra W, Blikman T, Mensink FB et al (2015) The modified painDETECT questionnaire for patients with hip or knee osteoarthritis: translation into Dutch, cross-cultural adaptation and reliability assessment. PLoS ONE 10:e0146117. https://doi.org/10.1371/journal.pone.0146117

Salo F, Nassif AB, Essex A (2019) Dimensionality reduction with IG-PCA and ensemble classifier for network intrusion detection. Comput Networks 148:164–175. https://doi.org/10.1016/j.comnet.2018.11.010

Sapra SK (2010) Robust vs. classical principalcomponent analysis in the presence of outliers. Appl Econ Lett 17:519–523. https://doi.org/10.1080/13504850802046989

Seczon L, Sagalovskiy A (2013) Field experience with the application and operation of permanent magnet motors in the ESP industry: success stories and lessons learned. In: SPE artificial lift conference-Americas. OnePetro. https://doi.org/10.2118/165030-MS

Singh A, Shukla A, Purwar S (2022) Leveraging machine learning and interactive voice interface for automated production monitoring and diagnostic. SPE Annu. Tech. Conf. Exhib. D021S038R003. https://doi.org/10.2118/210475-MS

Sophian A, Tian GY, Taylor D, Rudlin J (2003) A feature extraction technique based on principal component analysis for pulsed Eddy current NDT. NDT e Int 36:37–41. https://doi.org/10.1016/S0963-8695(02)00069-5

Stone P (2007) Introducing predictive analytics: Opportunities. In: Digital Energy conference and exhibition. OnePetro. https://doi.org/10.2118/106865-MS

Syed FI, Alshamsi M, Dahaghi AK, Neghabhan S (2022a) Artificial lift system optimization using machine learning applications. Petroleum 8:219–226. https://doi.org/10.1016/j.petlm.2020.08.003

Syed FI, Muther T, Dahaghi AK, Negahban S (2022b) Low-rank tensors applications for dimensionality reduction of complex hydrocarbon Reservoirs. Energy 244:122680. https://doi.org/10.1016/j.energy.2021.122680

Takacs G (2017) Electrical submersible pumps manual: design, operations, and maintenance. Gulf professional publishing

Teng W, Cheng L, Zhao K (2017) Application of kernel principal component and Pearson correlation coefficient in prediction of mine pressure failure. In: 2017 Chinese Automation Congress (CAC). IEEE, pp 5704–5708. https://doi.org/10.1109/CAC.2017.8243801

Thakur B, Samuel R (2021) Deep learning for downhole data prediction: a cost-effective data telemetry through data analytics. SPE West. Reg. Meet. D031S015R008. https://doi.org/10.2118/200870-MS

Vandevier J (2010) Run-time analysis assesses pump performance. Oil Gas J 108:76–79

Wang B, Han G, Lu X, et al (2022) Remote monitoring of well production performance based on machine learning. In: SPE western regional meeting. OnePetro. https://doi.org/10.2118/209255-MS